Biosensors and Bioelectronics 141 (2019) 111445

Contents lists available at ScienceDirect

Biosensors and Bioelectronics

journal homepage: www.elsevier.com/locate/bios

Ni–Fe PBA hollow nanocubes as efficient electrode materials for highly sensitive detection of guanine and hydrogen peroxide in human whole saliva

Qiangqiang Niu[a], Cancan Bao[a], Xiaowei Cao[b], Chang Liu[c], Hui Wang[a], Wenbo Lu[a,*]

[a] Key Laboratory of Magnetic Molecules and Magnetic Information Materials (Ministry of Education), School of Chemistry and Material Science, Shanxi Normal University, Linfen, 041004, China

[b] Institute of Translational Medicine, Medical College, Yangzhou University, Yangzhou, 225001, China

[c] State Key Laboratory of Bioelectronics, Southeast University, Nanjing, 210096, China

ARTICLE INFO

Keywords:
Ni-Fe
Prussian blue analogue
Hollow
Guanine
H_2O_2
Sensor

ABSTRACT

A sensor for the determination of guanine (G) and hydrogen peroxide (H_2O_2) is developed based on Ni–Fe Prussian blue analogues hollow nanocubes (Ni–Fe PBA HNCs) for the first time. As a remarkable redox probe towards G and H_2O_2 oxidation, Ni–Fe PBA HNCs exhibit a series of predominant sensing performances as follows: lower limit of detection, broader linear range and higher selectivity due to the homogeneous hollow structure, high specific surface and the enhanced electron transfer ability of Ni–Fe PBA HNCs. As a G sensor, it exhibits a wide linear range (0.05–4.0 mM) and a low detection limit of 0.0104 μM (S/N = 3). As a H_2O_2 sensor, the Ni–Fe PBA HNCs show superior sensing performances with a low detection limit of 0.291 μM (S/N = 3) and a wide detection range of 0.1–20 mM. By cause of these advantages, the real-time detection of G and H_2O_2 in human saliva are triumphantly accomplishment, indicating the applicability of Ni–Fe PBA HNCs.

1. Introduction

Ribonucleic acid (RNA) and deoxyribonucleic acid (DNA) are nucleic acids, which can constitute the major macromolecules essential for all known forms of life (Litke and Jaffrey, 2019; Monferrer et al., 2019). The guanine (G) is an important constituent part of RNA and DNA. G circulating in physiological fluids and tissues is related to the catabolism of DNA, the enzymatic degradation of tissues and the malfunction of enzymes (Wang et al., 2018; Ensafi et al., 2013). For this reason, changes in the concentration of G may portend the emergence of some diseases like HIV infection, diabetes and cancer (Pietrzyk et al., 2010). As a result, the determination of G in physiological fluids is of great significance. In addition, hydrogen peroxide (H_2O_2) is an important signaling molecule in the regulation of assorted biological processes (Veal et al., 2007; Gupta et al., 2018). H_2O_2 molecule is generated in response under the stimulation of some biological factors, such as cytokines, growth factors, and polymorphonuclear leukocytes (Veal et al., 2007; Gupta et al., 2018; Geiszt and Leto, 2004). It plays an important part in animal immune system and induces the cell damage through DNA base modifications (Lopa et al., 2018). Therefore, the exact determination of G and H_2O_2 is significant in biomedical and clinical diagnosis.

Prussian blue (PB) is a typical hexacyanoferrate coordination polymers, which formed by the linking of cyanogen and iron ions (Zakaria and Chikyow, 2017). PB has gained a great amount of interest in recent years, due to its extensive uses in lithium ion battery, sensors, water splitting and electrocatalysis (Zakaria and Chikyow, 2017; Lin et al., 2015; Wu et al., 2019; Han et al., 2016). Prussian blue analogues (PBAs) are composed of plural metal ions and cyanogen, which have received further research interests because of their higher specific surface areas, more catalytic active sites and lower potential transducer for electrocatalysis (Zakaria and Chikyow, 2017; Guo et al., 2018). The redox of plural metal ions that existed in PBAs can provide a channel for electrons (Indra et al., 2018). In the last few years, Various attempts have been made to synthesize nanostructured PBAs (Indra et al., 2018; Ahn et al., 2018; Zhang et al., 2018; Nai et al., 2017). Chen's group reported a ternary Ni–Co–Fe PBA for dual-electrocatalysis (Ahn et al., 2018). Nickel hexacyanoferrate PBA (Ni–Fe PBA) nanocubes as an active catalyst support are investigated by Zhang et al., (2018). Lou's group prepared the novel Ni–Fe PBAs and Ni–Co PBAs nanomaterials via a simple chemical route at room temperature (Han et al., 2016; Nai et al., 2017). The above-mentioned PBAs materials are mainly applied in the field of energy storage, but there are few reports in the literature describing PBAs materials used in sensing. Especially, PBAs hollow nanocubes as an electrocatalyst for H_2O_2 and G oxidation is no reported information.

* Corresponding author.
E-mail address: luwb@sxnu.edu.cn (W. Lu).

https://doi.org/10.1016/j.bios.2019.111445
Received 11 April 2019; Received in revised form 5 June 2019; Accepted 16 June 2019
Available online 25 June 2019

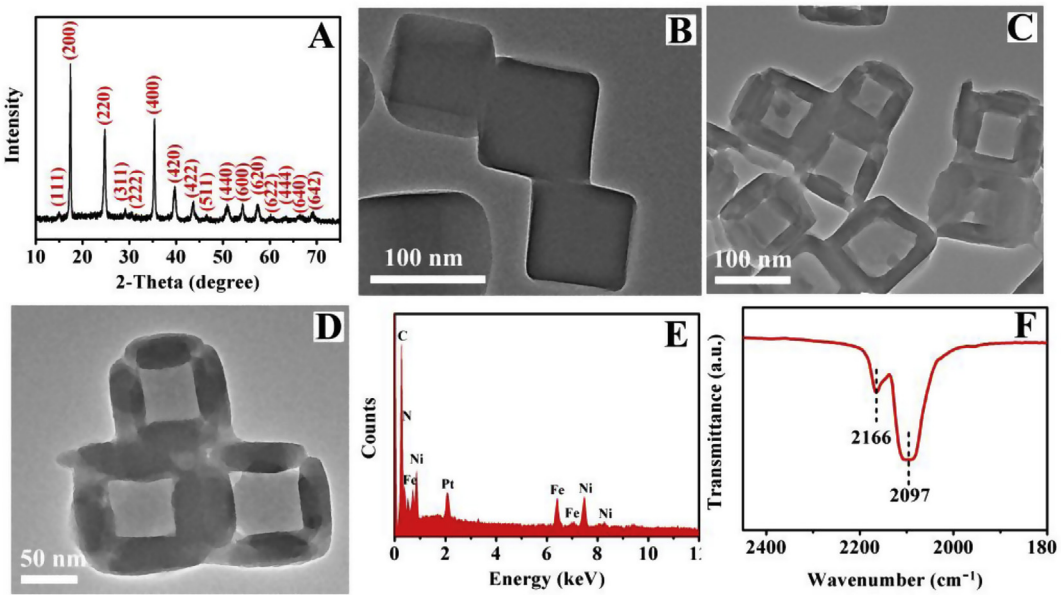

Fig. 1. (A) XRD pattern of Ni–Fe PBA HNCs; (B) TEM image of Ni–Fe PBA nanocubes; Low (C) and high (D) magnification TEM images of Ni–Fe PBA HNCs; (E) EDX spectrum of Ni–Fe PBA HNCs; (F) FT-IR spectrum of Ni–Fe PBA HNCs.

In this study, we describe our finding that Ni–Fe PBA hollow nanocubes (Ni–Fe PBA HNCs) exhibit high-efficiency electrocatalytic activity towards the oxidation of H_2O_2 and G in alkaline media. Furthermore, the synthesized Ni–Fe PBA HNCs are used as an electrochemical sensor for the high-performance detection of H_2O_2 and G molecules. As a G sensor, it exhibits excellent performance in detecting the concentration of G, with a wide linear range (0.05–4.0 mM) and a low detection limit of 0.0104 μM (S/N = 3). As a H_2O_2 sensor, the Ni–Fe PBA HNCs show superior sensing performances with a low detection limit of 0.291 μM (S/N = 3) and a wide detection range of 0.1–20 mM. By cause of these advantages, the real-time detection of H_2O_2 and G in human saliva are triumphantly accomplishment, indicating the applicability of Ni–Fe PBA HNCs. As a consequence, the Ni–Fe PBA HNCs could act as a hopeful candidate for application in biomedical field.

2. Experimental

2.1. Materials

H_2O_2 and $NH_3{\cdot}H_2O$ (28–30%) are purchased from Tianjin Guangfu Technology Development Co. Ltd. (Tianjin, China). Guanine, cytosine, thymine, adenine, glycine lysine, are purchased from Aladdin Co. Ltd. (Shanghai, China). Nickel(II) acetate, sodium citrate, potassium ferricyanide (III), potassium hexacyanoferrate (II), sodium hydroxide, sodium chloride, sodium sulfate, ferric trichloride (III), are purchased from Sinopharm Chemical Reagent Co. Ltd. (Shanghai, China). The above-mentioned reagents are used instantly without any pretreatment. The water used throughout all experiments is purified through a Millipore system. The human saliva samples are kindly provided by graduate students of our group in Shanxi Normal University (Linfen, China).

2.2. Preparation of Ni–Fe PBA hollow nanocubes

Ni–Fe PBA HNCs are obtained by chemical etching method of Ni–Fe PBA nanocubes (Nai et al., 2017). Ni–Fe PBA nanocubes as precursor is firstly synthesized in this work, the detailed synthesis process is as follows: A mixed solution (c solution) is obtained by 80 mL of deionized (DI) water containing 0.60 g of nickel(II) acetate tetrahydrate, 0.882 g of trisodium citrate dihydrate (a solution) and 120 mL of DI water with 0.528 g of potassium hexacyanoferrate(III) (b solution). When solution b is slowly added into solution a, it's worth noting that the mixed solution (c solution) is stirring in whole process and continuous stirring for another 1 min. Then, the c solution is aged for 1 day at room temperature. By two stage centrifugations (first 4000 r/min to remove the large particles and then 9000 r/min for 6 min, respectively) to collect precipitates, with DI water and ethanol to wash precipitates three times, respectively. Finally, the Ni–Fe PBA nanocubes are dried at 75 °C for 10 h.

Ni–Fe PBA HNCs are prepared as follows: 20 mg of the as-prepared Ni–Fe PBA nanocubes are dispersed into 10 mL of ethanol. Following a mixed solution of 20 mL of H_2O containing 5 mL of $NH_3{\cdot}H_2O$ (28 ~ 30%) is added into the above dispersion solution with stirring for 5 min at room temperature. The ammonia plays a cavity producer role in the cube-to-hollow cube conversion process. The cavity is formed which based on the react between ammonia and Ni(II)-N≡C–Fe(III), corresponding equation as follows:

$$Ni_3^{II}[Fe^{III}(CN)_6]_2 + 18NH_3 \rightarrow 3[Ni(NH_3)_6]^{2+} + 2[Fe(CN)_6]^{3-}$$

The precipitates (Ni–Fe PBA HNCs) are collected by centrifugation with 9000 r/min for 6 min, with DI water and ethanol to wash precipitate three times and dried at 75 °C for 10 h.

3. Results and discussion

3.1. Characterization of Ni–Fe PBA HNCs

The crystal structure of the Ni–Fe PBA HNCs are characterized by X-ray diffraction (XRD) measurements. Fig. 1A shows the XRD pattern of the synthesized Ni–Fe PBA HNCs. These peaks located at 14.9°, 17.2°, 24.5°, 28.8°, 30.1°, 35.0°, 39.3°, 43.3°, 46.0°, 50.4°, 53.6°, 56.8°, 65.6° and 68.65° can be indexed to the (111), (200), (220), (311), (222), (400), (420), (422), (511), (440), (600), (620), (640) and (642) crystal planes of Ni–Fe PBA HNCs, respectively (Bu et al., 2018). All of diffraction peaks exhibit a typical Prussian blue analog-type pattern with the face-centered cubic structure (Nai et al., 2017).

Fig. 1B shows the transmission electron microscopy (TEM) image of Ni–Fe PBA nanocubes. It is clearly seen that the nanoparticles of Ni–Fe PBA nanocubes have a cubic structure and the average diameter is

about 111 nm. The TEM images of Ni–Fe PBA HNCs make a display in Fig. 1C and D, compared to Fig. 1B, the hollow structure can be obviously observed. According to the TEM images, the diameter is approximatively 111 nm and the pore size is mainly distributed in 37–50 nm. In addition, the pore size and specific surface area of the Ni–Fe PBA HNCs material are studied by Brunauer–Emmett–Teller (BET) method, as shown in Fig. S1 (Supplementary Materials). BET surface area is 92.7981 $m^2 g^{-1}$ based on the nitrogen adsorption-desorption isotherms. The pore size is mainly distributed in the range of 20–50 nm, as shown in inset of Fig. S1(Supplementary Materials). Fig. 1E shows the energy-dispersive X-ray (EDX) spectrum exhibits the presence of Ni, Fe, C, and N elements in the composites, which are originated from nickel(II) acetate and potassium hexacyanoferrate(III). The Ni and Fe content of Ni–Fe PBA HNCs are calculated by Inductively coupled plasma atom emission spectrometry (ICP-AES) technology, indicating that the amount of Ni:Fe ratio is 3:1. The X-ray photoelectron spectrum (XPS) survey of the Ni–Fe PBA HNCs further confirms the presence of Ni, Fe, C and N elements in product, as shown in Fig. S2. The TEM mapping patterns of Ni–Fe PBA HNCs are characterized by TEM technology at the voltage of 120 kV. The TEM mapping of Ni–Fe PBA HNCs indicate that the elements of Ni and Fe are evenly spread all over the entire hollow nanocube in Fig. S3. The Fourier transform infrared (FT-IR) spectrum of the Ni–Fe PBA HNCs is displayed in Fig. 1F. Two bands at 2166 cm^{-1} and 2097 cm^{-1} are corresponding to the Ni (II)–N≡C–Fe(III) and Ni(II)–N≡C–Fe(II) species, respectively (Sato et al., 1996). All these above observations confirm that the Ni–Fe PBA HNCs have been prepared successfully.

3.2. Non-enzyme G sensor based on Ni–Fe PBA HNCs

The synthesized Ni–Fe PBA HNCs are immediately employed as G sensing electrode. Fig. 2A shows that the electrocatalytic behavior of related modified electrodes have been investigated using cyclic voltammetry (CV) technique, 0.1 M NaOH (pH: 13) solution as a supporting electrolyte. The potential range is -0.3–0.8 V in the CV test. The Nafion decorated glassy carbon electrode (Nafion/GCE) and bare GCE exhibit no peaks in 0.1 mM G solution. While the Ni–Fe PBA HNCs/Nafion/GCE exhibits an obvious oxidation peak in the presence of 0.1 mM G compared with the Nafion/GCE or bare GCE. Under the same test conditions, Ni PBA HNCs/Nafion/GCE and Fe PBA HNCs/Nafion/GCE exhibit an oxidation peak. Compared with the Ni–Fe PBA HNCs/Nafion/GCE, the peak current value of them are obviously weakened. These results prove that Ni–Fe PBA HNCs/Nafion/GCE possesses the desirable electro-catalytic ability towards G oxidation. In the absence of G, the Ni–Fe PBA HNCs/Nafion/GCE shows an obvious oxidation peak (red line b), which can be attributed to the conversion of Ni(II) and Ni (III) in the Ni–Fe PBA HNCs. However, a notable enhancement of peak current occurs in the present of 0.1 mM G because the oxidation of G enhances the current. The proposed mechanism of G oxidation could be interpreted by the following reactions:

$$Ni(II)–N\equiv C–Fe(III) \rightarrow Ni(III)–N\equiv C–Fe(III) + e-$$

$$Ni(III)–N\equiv C–Fe(III) + G + H2O \rightarrow Ni(II)–N\equiv C–Fe(III) + \text{the oxidation of } G + e- + H+$$

According to the preceding reactions, the Ni(II)–N≡C–Fe(III)/Ni (III)–N≡C–Fe(III) redox couple can catalyze the oxidation of G, emerging an enhancement in anodic peak current. These observations confirm that Ni–Fe PBA HNCs is efficient for G electro-oxidation.

On average, we can acquire some essential information which involved in the electrochemical reaction mechanism according to the linear function of peak current (I) and scan rate (ν). Consequently, we recorded the influence of the scan rate on the oxidation susceptibility of Ni–Fe PBA HNCs/Nafion/GCE towards G. Fig. 2B records the CV response of 0.1 mM G solution at unequable scan rates. With the increase of scanning speed, the peak current step by step increased. The relation between peak current and scan rate is expressed in regression equations: (1) oxidation peak: Ipa (μA) = 0.1585ν (mV s^{-1}) + 3.2739 (R^2 = 0.999) and (2) reduction peak: Ipc (μA) = −0.1057ν (mV s^{-1}) + 0.0034 (R^2 = 0.993), as shown in inset of Fig. 3B. It proves that the oxidation of G on Ni–Fe PBA HNCs/Nafion/GCE is an adsorption controlling process.

The amount of G adsorbed on the surface of Ni–Fe PBA HNCs/Nafion/GCE can be calculated based on the following equation (Laviron, 1974):

$$I_p = nFAQ\nu / 4RT = n^2F^2A\nu\Gamma_c / 4RT. \ (Q = nFA\Gamma_c)$$

The symbolic meaning of each letter involved in the equation as

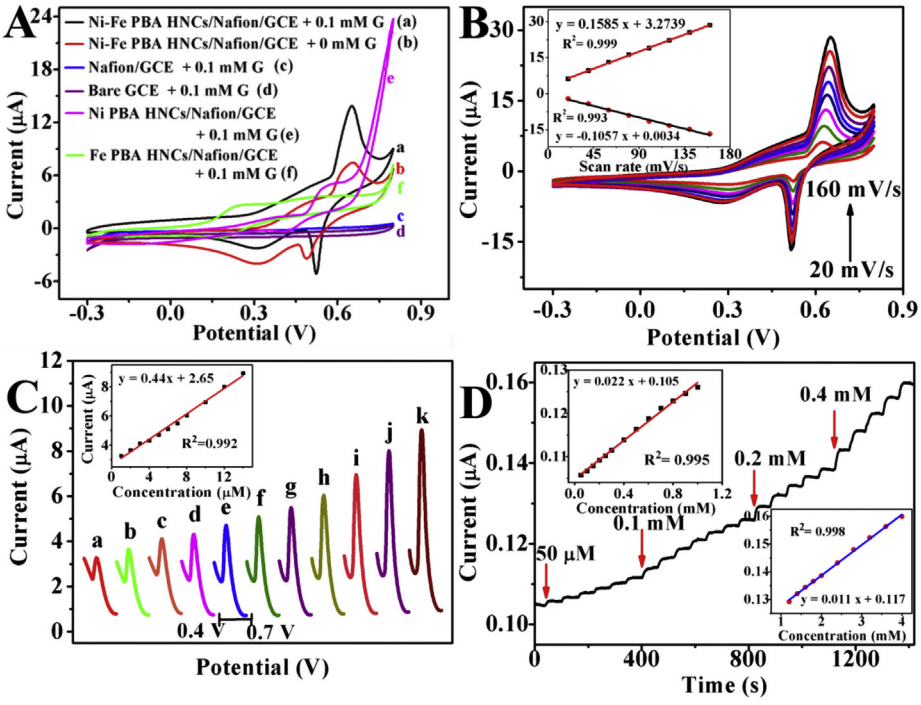

Fig. 2. In 0.1 M NaOH electrolyte: (A) CV curves for the Ni–Fe PBA HNCs/Nafion/GCE, Nafion/GCE, Bare GCE, Ni PBA HNCs/Nafion/GCE and Fe PBA HNCs/Nafion/GCE with the presence (black line a, blue line c, purple line d, pink line e and green line f) and absence (red line b) of 0.1 mM G (scan rate: 50 mV/s). (B) CV curves of the Ni–Fe PBA HNCs/Nafion/GCE obtained at scan rates from 20 to 160 mV/s in 0.1 mM G (Inset: anodic and cathodic peak current as a linear function of scan rates). (C) DPV curves for the Ni–Fe PBA HNCs/Nafion/GCE with the presence varying concentrations of G, potential range: 0.4 ~ 0.7 V, where G concentrations are 0.1, 0.2, 0.3, 0.4, 0.5, 0.6, 0.7, 0.8, 1.0, 1.2 and 1.4 mM, respectively. (D) i-t curve of Ni–Fe PBA HNCs/Nafion/GCE to consecutive addition of G into a stirring electrolyte solution at 0.65 V (inset: the linear function of peak current versus concentrations). (For interpretation of the references to colour in this figure legend, the reader is referred to the Web version of this article.)

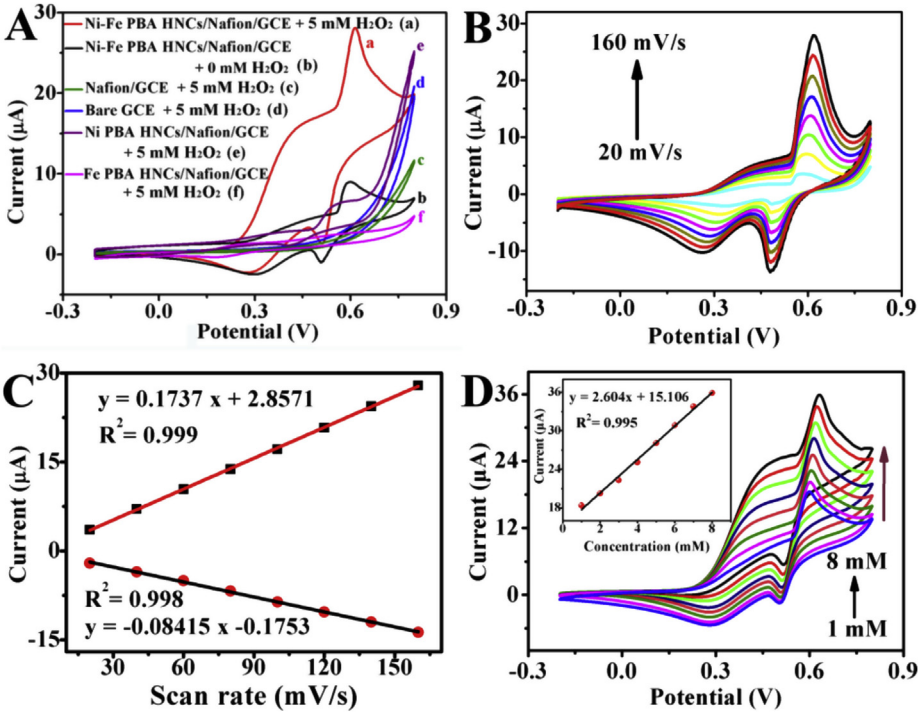

Fig. 3. (A) CV curves of bare GCE, Nafion/GCE, Ni PBA HNCs HNCs/Nafion/GCE, Fe PBA HNCs HNCs/Nafion/GCE and Ni–Fe PBA HNCs/Nafion/GCE in 0.1 M NaOH with and without 5.0 mM H_2O_2, separately (scan rate: 50 mV/s); (B) CV curves of the Ni–Fe PBA HNCs/Nafion/GCE in 0.1 M NaOH solution containing 3 mM H_2O_2 at various scan rates ranging from 20 to 160 mV/s; (C) Plot of oxidation peak current (Ipa) and reduction peak current (Ipc) versus scan rate, respectively; (D) CVs of the Ni–Fe PBA HNCs/Nafion/GCE with variant concentrations of H_2O_2 from 1 mM to 8 mM in 0.1 M NaOH electrolyte, scan rate: 50 mV/s (Inset: the calibration plot of the peak current responses to the corresponding H_2O_2 concentration).

follows: n presents the number of transfer transport, F is Faraday's constant (F = 96,500 C mol^{-1}), A is the area of the work electrode, Γ_c is the adsorption capacity of G on the surface of Ni–Fe PBA HNCs/Nafion/GCE, Q is the quantity of charge consumed during the electrooxidation reaction, and v is the scanning speed. In the linear relationship between Ipa and v, its slope is equal to 2.303RT/(1-α)nF, (α: electron transfer coefficient, n: the number of the transferred electrons). In consequence, we calculated that the transfer transport number is 1 for the electrooxidation of G, when the value of α for the irreversible reaction is assumed to be 0.5. According to the above equation, the adsorption capacity of G on the surface of Ni–Fe PBA HNCs/Nafion/GCE (Γ_c) is obtained to be 7.59×10^{-7} mol cm^{-2}.

Above results suggest that the Ni–Fe PBA HNCs as a 3D catalyst for nonenzymatic G sensing is feasible. Next, we explore the electrochemical behaviors of Ni–Fe PBA HNCs/Nafion/GCE towards different concentrations of G in electrolyte solution. Differential pulse voltammetry (DPV) curves obtained by various concentrations of G with peak currents are shown in Fig. 2C. The oxidation current near 0.65 V of the Ni–Fe PBA HNCs/Nafion/GCE strengthened gradually with the increasing of G in a larger concentration range from 0.1 to 1.4 mM. In inset of Fig. 2C, the linear regression equation constructed by oxidation peak current and the concentration of G (R^2 = 0.992) indicates that the current is linearly associated with the concentration. At constant potential of 0.65 V, the chronoamperometric response towards successive injection of certain amounts of G is shown in Fig. 2D, this measure makes further efforts to corroborate the excellent electrocatalytic performance of Ni–Fe PBA HNCs. It is clearly seen that a well-defined response is observed during successive additions of G, demonstrating the stable and efficient catalytic property of the immobilized electrocatalyst. An instant increase in the current is observed immediately after addition of G and a stable state reaches within 10 s.

The plot of the current response vs G concentration is shown in inset of Fig. 2D. Dependence of the peak current on G concentration in the ranges of 0.05 ~ 1.0 and 1.0 ~ 4.0 mM are linear with regression equations of I (μA) = 0.022 C (mM) + 0.105 and I (μA) = 0.011C (mM) + 0.117. The values of R^2 are 0.995 and 0.998, respectively. These linear equations indicate that the regression lines are fitted very well with the experimental data, and can be applied for the determination of the substances in unknown samples. The limit of detection is found to be 0.0104 μM based on signal-to-noise factor of 3. The sensitivity on the modified electrode for G is 1.708 μA mM^{-1} cm^{-2}. These results are also compared with other sensors used for G detection, as listed in Table S1. Definitely, the Ni–Fe PBA HNCs/Nafion/GCE acquires super analytical performance than reported sensors. As a result, the Ni–Fe PBA HNCs can be constructed a sensing platform, which provides a convenient and quick testing tool for the determination of G.

3.3. Non-enzyme H_2O_2 sensor based on Ni–Fe PBA HNCs

The Ni–Fe PBA HNCs are also employed as H_2O_2 sensing electrode due to the persistent transformation between Ni(II), Fe(II) and Ni(III), Fe(III) redox pairs. This experiment is carried out in a typical three-electrode system: a platinum wire is served as the auxiliary electrode, Ag/AgCl (saturable KCl) is acted as the reference electrode, and a GCE modified with Ni–Fe PBA HNCs plays a role in the working electrode. To assess the electro-catalyst property of the Ni–Fe PBA HNCs toward H_2O_2, CV experiments of GCE, Nafion/GCE and Ni–Fe PBA HNCs/Nafion/GCE with and without H_2O_2 in 0.1 M NaOH solution are performed in Fig. 3A. The oxidation peak current enhances obviously when the GCE surface is modified with Ni–Fe PBA HNCs (curve a and b), while bare GCE has no typical characteristic peak (curve d), manifesting no catalytic performance for H_2O_2. The current hardly changed yet after Nafion is decorated onto GCE surface in 5 mM H_2O_2 (curve c), which indicates that Nafion not only does not hinder the transfer of electrons between electrode and analyte, but also plays a role in conducting and fixing here as a mediator.

Other modified electrodes with Ni PBA HNCs and Fe PBA HNCs exhibit weak oxidation peak in 5 mM H_2O_2 (curve e and curve f), which suggest that the weaker electrooxidation activity to H_2O_2 compared with the Ni–Fe PBA HNCs electrode (curve a). For the Ni–Fe PBA HNCs/Nafion/GCE, a weak electrochemical response signal is examined in the absence of H_2O_2 (curve b). We can draw a conclusion that the oxidation peak is located in 0.60 V, which attributes to the reason that Ni(II) is oxidized to Ni(III) at this potential. The reduction peak situated at 0.51 V could be treated as a process of Ni(III)/Fe(III) is reduced to Ni (II)/Fe(II) on the basic of the published reference (Tao et al., 2018; Li

et al., 2009). On the contrary, a quasi-reversible redox couple can be apparently noticed, and noticeable peaks current respond are measured both the anode and the cathode at 0.61 V and 0.51 V separately in 0.1 M alkaline solution containing 5 mM H_2O_2. The oxidation of Ni (II)–N≡C–Fe(III) takes place and Ni(II)–N≡C–Fe(III) is converted into Ni(III)–N≡C–Fe(III) on the prepared sensor. Meanwhile, the reaction that H_2O_2 oxidized to oxygen gas is underway simultaneously with the reducing reaction of Ni(III)/Fe(III) during the catalytic process, which causes an eminent enhancement of peak current in red line of Fig. 3A. It is proved that the extraordinary electro-oxidation behavior of the Ni–Fe PBA HNCs towards H_2O_2.

To investigate the electron transfer behavior of the Ni–Fe PBA HNCs/Nafion/GCE, Fig. 3B shows CVs of the sensor in 3 mM H_2O_2 solution are presented with variant scan rates of 20 ~ 160 mV/s. As the scanning speed raises continually, the currents of anode and cathode also gradually strengthen. It is further found that the redox peak currents are linearly dependent on the scan rates. As shown in Fig. 3C, I_{pa} has an outstanding relevant correlation with ν, and its linear relationship equation can be stated as:

$$I_{pa}\ (\mu A) = 2.8571 + 0.1737\ \nu\ (mV/s)\ (R^2 = 0.999)$$

I_{pc} also has an analogical linear correlation with ν, and its relevant correlation equation can be demonstrated as:

$$I_{pc}\ (\mu A) = -0.1753–0.08415\ \nu\ (mV/s)\ (R^2 = 0.998)$$

The relevance demonstrating that the redox reaction of H_2O_2 on the Ni–Fe PBA HNCs-modified electrode is a typical surface-controlled process (Huang et al., 2017). Based on the Laviron theory (Laviron, 1974), we can receive the quantity of electron transport on the Ni–Fe PBA HNCs/Nafion/GCE according to the etymology of electricity, which can be figured out from CV peak area in a random scanning speed. As a result, we can draw a conclusion that the number of transferred electrons is equal to 2. Fig. 3D displays the CVs of the Ni–Fe PBA HNCs/Nafion/GCE by adding distinct concentrations from 1 mM to 8 mM of H_2O_2 into NaOH solution (pH = 13). It is found that the oxidation peak current enhances step by step, with the increase of H_2O_2 concentration. Moreover, calibration plot corresponding to current response (the inset of Fig. 3D) is linear over the concentrations of H_2O_2 ranging from 1.0 to 8.0 mM (R^2 = 0.995).

Based on preceding comments, we can expound the process of electro-catalytic oxidation of H_2O_2 by Ni–Fe PBA HNCs as follows (Tao et al., 2018; Li et al., 2009):

$$Ni(II)–N{\equiv}C–Fe(III) \rightarrow Ni(III)–N{\equiv}C–Fe(III) + e- \quad (1)$$

$$Ni(III)–N{\equiv}C–Fe(III) + H_2O_2 + e- \rightarrow Ni(II)–N{\equiv}C–Fe(III) + O_2\uparrow \quad (2)$$

$$Ni(II)–N{\equiv}C–Fe(III) + H_2O_2 \rightarrow Ni(II)–N{\equiv}C–Fe(II) + 2H^+ + O_2\uparrow \quad (3)$$

From these above formulas, we conclude that the electro-catalysis of H_2O_2 emerges oxygen gas increasing gradually on the electrode surface with the successive influxion of H_2O_2, giving rise to a perceptible enlargement in oxidation peak current eventually (Yan et al., 2012).

The catalytic abilities of different potentials for H_2O_2 response are discriminatory. In order to gain the most suitable potential for H_2O_2 detection, we recorded the amperometric response of 0.2 mM H_2O_2 consecutively injected into 0.1 M NaOH electrolyte at varying anode potentials of 0.58 ~ 0.62 V (Fig. 4A). The inset of Fig. 4A reveals the calibration curves of the relationship between peak current and corresponding concentration at different potentials, we can draw a conclusion that the potential of 0.61 V is selected as the favorable potential because of the highest current response. As displayed in Fig. 4B, the characteristic amperometric response to the consecutive influxion of various concentrations of H_2O_2 into the 0.1 M NaOH solution at a constant potential of 0.61 V. It is discovered that the amperometric current responds quickly to the H_2O_2 and achieves the stable state within 8 s with various concentrations of H_2O_2, indicating the rapid absorption and activation of H_2O_2 on the electrode surface. Fig. 4C reveals the plot of amperometric response to distinct concentrations of H_2O_2 in 0.1 M NaOH solution. We can conclude that the correlative linear range for the H_2O_2 detection is 0.1 ~ 20 mM. Moreover, the detection limit of the Ni–Fe PBA HNCs/Nafion/GCE towards the H_2O_2 is calculated as 0.291 μM (S/N = 3), RSD = 8.8%. As H_2O_2 sensor, the sensitivity on the modified electrode is 36.13 μA mM^{-1} cm^{-2}. The H_2O_2 sensor exhibits a lower limit of detection and broader linear range compared with other reported similar electrochemical H_2O_2 sensors, as shown in Table S2, demonstrating a promising prospect in real applications. Fig

The excellent sensing performance of Ni–Fe PBA HNCs/Nafion/GCE is reflected principally as following: Firstly, the typical characteristic of Ni–Fe PBA HNCs, including the controlled homogeneous hollow nanotube structure, high specific surface and tiny cube diameter size about 111 nm, which be able to reveal more reactive spots and supply a more responsive approach for mass transfer and charge transfer processes to accelerate the reaction going on (Xiang et al., 2015). Schematic diagram of electron transmission is shown in Fig. S4. Secondly, the fore-mentioned individual construction probable as well benefit the rapid overflow of oxygen generated by the oxidation of H_2O_2 in the electro-oxidation process (Zhan et al., 2018). Finally, the coreless fabric nanocubes possess more reactive sites and convenient transfer channels for H^+ and electron between the electrode and the electrolyte interface (Tao et al., 2018).

Selectivity is another essential research object in the study of electrochemical sensor in actual applications. Therefore, we exploit the amperometric response of the Ni–Fe PBA HNCs/Nafion/GCE in the presence of different interferents (1.0 mM) to clarify the influence on H_2O_2. As shown in Fig. 4D, the prepared sensor presents especially glorious response for H_2O_2 electro-oxidation, however the signal change of the interfering substances is hardly observable for the 2-fold concentrations of lysine, glycine, chloride ion (Cl^-), sulfate ion (SO_4^{2-}), cytosine (C), adenine (A) and thymine at a working potential of 0.61 V, demonstrating the electrode has superior anti-interference ability. The perfect selectivity of Ni–Fe PBA HNCs may be ascribed to the optimized potential for H_2O_2 electrocatalysis, where other interfering substances cannot cause the electrochemical reaction procedure to go on. Fig. S5 shows the long-period stability of the Ni–Fe PBA HNCs/Nafion/GCE is also investigated in our study. The sensor response to H_2O_2 is measured within 30 days. We stored the sensor in the air and performed a CV test every 5 days to record the change in peak current value. The result shows that the current signal is 92.1% of its original signal after 30 days of storage (I/I_0 = 92.1%), indicating that the G sensor based on Ni–Fe PBA HNCs has a good stability for H_2O_2 detection.

3.4. Detection of G and H_2O_2 in real sample

For the sake of determine the feasibility of the enzyme-free H_2O_2 sensor in practice use, the human saliva samples are spiked with a stream of concentrations H_2O_2 and tested by the CV method on Ni–Fe PBA HNCs/Nafion/GCE. Fig. 5 presents that the oxidation peak current increase with continuous injection of H_2O_2 into the human saliva sample. The corresponding calibration curve (I (μA) = 1.91C (mM) + 22.30, R^2 = 0.996, RSD = 5.52%) indicates that the peak current increase linearly with increased H_2O_2 concentrations ranging from 0 to 8 mM. It would be powerful enough to prove that our sensor can be used for the detection of H_2O_2 in real samples.

The authenticity of the nonenzymatic sensor with Ni–Fe PBA HNCs/Nafion/GCE is further verified by recovery study of analytes in real samples. For G and H_2O_2 determination, saliva samples are used as real sample which obtained from normal human body, centrifuged at 9000r/min for 10 min without any additional pretreatment, collected supernatant and stored at 4 °C for standby application. The recovery study of analytes by CV technology, whole saliva as supporting

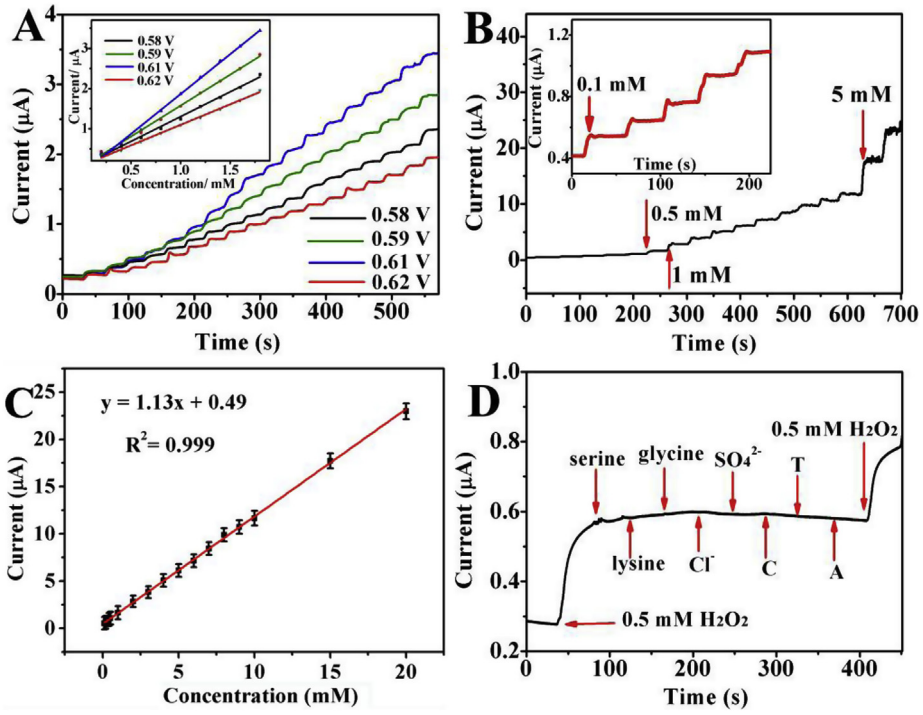

Fig. 4. (A) Amperometric response of Ni–Fe PBA HNCs/Nafion/GCE for successive injection of H_2O_2 with different concentrations at disparate working potentials. (Inset: the corresponding calibration curves). (B) Amperometric response to the varied concentrations of H_2O_2 poured into NaOH solution consecutively at 0.61 V. (C) Plot of amperometric response to different concentrations of H_2O_2. (D) i-t curve with the inpouring of H_2O_2 (0.5 mM) and various interfering compounds (1 mM, serially) in 0.1 M NaOH at an immobile potential of 0.61 V.

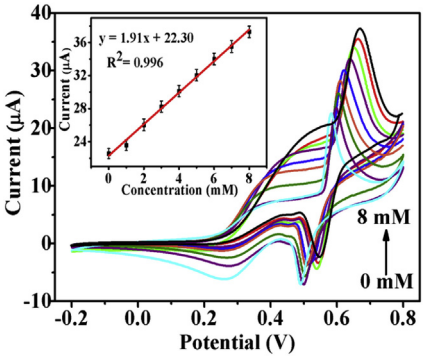

Fig. 5. CV curves for the Ni–Fe PBA HNCs/Nafion/GCE in a human whole saliva sample with the presence of different H_2O_2 concentrations from 0 to 8 mM at a scan rate of 50 mV/s (Inset: the corresponding linear calibration curve).

electrolyte. The amount tested by sensor are compared with practical added amount, and the recovery rates are calculated for G and H_2O_2, respectively, as shown in Table S3 and Table S4. It can be seen from the table that the acceptable recoveries of G and H_2O_2 indicate the sensor we prepared possess good availability in real saliva samples.

4. Conclusions

The Ni–Fe PBA HNCs have been proven as an efficient electrocatalyst for G and H_2O_2 oxidation. The sensor based on Ni–Fe PBA HNCs can be used for the simultaneous detection of G and H_2O_2 in real samples. As a non-enzymatic sensor, it exhibits lower limit of detection, broader linear range and higher selectivity. Our present work can be used to provide a magnetic and low-cost hybrid materials for applications in various types of chemical sensors and biosensors.

Declaration of interest statement

We declare that we have no financial and personal relationships with other people or organizations that can inappropriately influence our work, there is no professional or other personal interest of any nature or kind in any product, service and/or company that could be construed as influencing the position presented in, or the review of, the manuscript entitled.

CRediT authorship contribution statement

Qiangqiang Niu: Writing - original draft, Formal analysis, Writing - review & editing. **Cancan Bao:** Writing - original draft, Writing - review & editing. **Xiaowei Cao:** Writing - original draft, Formal analysis. **Chang Liu:** Writing - original draft, Formal analysis. **Hui Wang:** Writing - original draft. **Wenbo Lu:** Writing - original draft, Formal analysis, Writing - review & editing, Supervision, Funding acquisition.

Acknowledgements

This work is supported by the National Natural Science Foundation of China (No.21705103), the Applied Basic Research Project of Shanxi Province (No. 201801D221392), the Graduate Education Innovation Project of Shanxi Province (2018SY057), Collaborative Innovation Center for Shanxi Advanced Permanent Materials and Technology and the 1331 Engineering of Shanxi Province. We appreciate Prof. Dr. Xiufang Qin (Shanxi Normal University) for her help on TEM and XRD characterizations.

Appendix A. Supplementary data

Supplementary data related to this article can be found at https://doi.org/10.1016/j.bios.2019.111445.

References

Ahn, W., Park, M.G., Lee, D.U., Seo, M.H., Jiang, G., Cano, Z.P., Hassan, F.M., Chen, Z., 2018. Adv. Funct. Mater. 28, 1802129.
Bu, F., Chen, W., Gu, J., Agboola, P.O., Al-Khalli, N.F., Shakir, I., Xu, Y., 2018. Chem. Sci. 9, 7009–7016.
Ensafi, A.A., Jafari-Asl, M., Rezaei, B., Allafchian, A.R., 2013. Sensor. Actuator. B Chem. 177, 634–642.
Geiszt, M., Leto, T.L., 2004. J. Biol. Chem. 279, 51715–51718.
Guo, Y., Tang, J., Wang, Z., Sugahara, Y., Yamauchi, Y., 2018. Small 14, 1802442.

Gupta, R., Singh, P., Ganesan, V., Koch, B., Rastogi, P.K., Yadav, D.K., Sonkar, P.K., 2018. Sensor. Actuator. B Chem. 276, 517–525.
Han, L., Yu, X.Y., Lou, X.W., 2016. Adv. Mater. 28, 4601–4605.
Huang, M., Luo, X., He, D., Jiang, P., 2017. Anal. Methods 9, 5903–5909.
Indra, A., Paik, U., Song, T., 2018. Angew. Chem. Int. Ed. 57, 1241–1245.
Laviron, E., 1974. J. Electroanal. Chem. Interfacial Electrochem. 52, 355–393.
Li, J., Wei, X., Yuan, Y., 2009. Sensor. Actuator. B Chem. 139, 400–406.
Lin, Y., Hu, L., Yin, L., Guo, L., 2015. Sensor. Actuator. B Chem. 210, 513–518.
Litke, J.L., Jaffrey, S.R., 2019. Nat. Biotechnol. https://doi.org/10.1038/s41587-019-0090-6.
Lopa, N.S., Rahman, M.M., Ahmed, F., Sutradhar, S.C., Ryu, T., Kim, W., 2018. Electrochim. Acta 274, 49–56.
Monferrer, A., Zhang, D., Lushnikov, A.J., Hermann, T., 2019. Nat. Commun. 10, 608.
Nai, J., Lu, Y., Yu, L., Wang, X., Lou, X.W., 2017. Adv. Mater. 29, 1703870.
Pietrzyk, A., Suriyanarayanan, S., Kutner, W., Chitta, R., Zandler, M.E., D'Souza, F., 2010. Biosens. Bioelectron. 25, 2522–2529.
Sato, O., Iyoda, T., Fujishima, A., Hashimoto, K., 1996. Science 272, 704–705.
Tao, Y., Chang, Q., Liu, Q., Yang, G., Guan, H., Chen, G., Dong, C., 2018. Surf. Interface 12, 102–107.
Veal, E.A., Day, A.M., Morgan, B.A., 2007. Mol. Cell 26, 1–14.
Wang, D., Huang, B., Liu, J., Guo, X., Abudukeyoumu, G., Zhang, Y., Ye, B.-C., Li, Y., 2018. Biosens. Bioelectron. 102, 389–395.
Wu, Z., Xie, J., Xu, Z.J., Zhang, S., Zhang, Q., 2019. J. Mater. Chem. A. 7, 4259–4290.
Xiang, D., Yin, L., Ma, J., Guo, E., Li, Q., Li, Z., Liu, K., 2015. Analyst 140, 644–653.
Yan, Q., Wang, Z., Zhang, J., Peng, H., Chen, X., Hou, H., Liu, C., 2012. Electrochim. Acta 61, 148–153.
Zakaria, M.B., Chikyow, T., 2017. Coord. Chem. Rev. 352, 328–345.
Zhan, T., Kang, J., Li, X., Pan, L., Li, G., Hou, W., 2018. Sensor. Actuator. B Chem. 255, 2635–2642.
Zhang, X., Liu, P., Sun, Y., Zhan, T., Liu, Q., Tang, L., Guo, J., Xia, Y., 2018. Inorg. Chem. Front. 5, 1683–1689.